International Journal of Nanomedicine

Dovepress

open access to scientific and medical research

Open Access Full Text Article

ORIGINAL RESEARCH

Glyconanoparticles with Activatable Near-Infrared Probes for Tumor-Cell Imaging and Targeted Drug Delivery

Guanyu Chi*, Yinghua Lv*, Shuang Chao*, Chenxi Hou, Yuxin Pei, Zhichao Pei

Shaanxi Key Laboratory of Natural Products and Chemical Biology, College of Chemistry and Pharmacy, Northwest A&F University, Yangling, Shaanxi, 712100, People's Republic of China

*These authors contributed equally to this work

Correspondence: Zhichao Pei, Shaanxi Key Laboratory of Natural Products and Chemical Biology, College of Chemistry and Pharmacy, Northwest A&F University, Yangling, Shaanxi 712100, People's Republic of China, Tel/Fax +86 29 8709-2769, Email peizc@nwafu.edu.cn

Background: Multifunctional nanocarriers based on tumor targeting and intracellular monitoring have received much attention and been a subject of intensive study by researchers in recent years. In this study, we report multifunctional glyconanoparticles with activatable near-infrared probes for tumor imaging and targeted drug delivery.

Methods: Disulfide-functionalized dicyanomethylene-4*H*-pyran (DCM-SS-NH_2) and amino-functionalized lactose were modified and loaded onto the surfaces of polydopamine nanoparticles (NPs) by Michael addition or Schiff-base reaction as GSH stimulation–responsive fluorescent probes and tumor-targeting moieties, respectively. Doxorubicin (DOX), a model anticancer drug, was loaded onto polydopamine through π–π interactions directly to prepare multifunctional PLDD (PDA@Lac/DCM/DOX) NPs.

Results: Experimental results showed that PLDD NPs had been successfully prepared. DCM, the fluorescence of which was quenched in PLDD NPs, was able to restore red fluorescence in a solution with a GSH concentration of 5 mM. The amount of DOX released from PLDD NPs was 44% over 72 hours in a weak-acid environment (pH 5). The results of CLSM and flow cytometry indicated that the PLDD NPs had good HepG2-targeting ability due to the special recognition between lactose derivative of NPs and overexpressed asialoglycoprotein receptors on HepG2 cell membrane. More importantly, the disulfide bond of DCM-SS-NH_2 was broken by the high concentration of GSH inside cancer cells, activating the near-infrared fluorescence probe DCM for cancer-cell imaging. MTT assays indicated that PLDD NPs exhibited higher anticancer efficiency for HepG2 cells and had reduced side effects on normal cells compared with free DOX.

Conclusion: The fluorescence of modified DCM loaded onto PLDD NPs is able to be restored in the high-concentration GSH environment within cancer cells, while improving the effectiveness of chemotherapy with reduced side effects. It provides a good example of integration of tumor imaging and targeted drug delivery.

Keywords: near-infrared probes, targeted drug delivery, GSH-responsive, tumor-cell imaging, polydopamine

Introduction

Multifunctional nanocarriers based on tumor targeting and intracellular monitoring have received much attention and been a subject of intensive study by researchers in recent years. Imaging-guided nanomedicine driven by precision medicine makes it possible to observe processes by microscopy at nanometer scale for widespread application in the diagnosis and treatment of cancer.[1–6] At present, near-infrared (NIR) fluorescent dyes are paving the way for the development of bioimaging technology because of their NIR absorption/emission wavelength, high sensitivity, and low biotoxicity.[7–10] Many NIR fluorescent probes for cancer-cell monitoring and tumor-tissue localization have been reported to successful.[11,12] However, although probes using small molecules are easy to synthesize and are taken up readily by cells, their development is limited by such disadvantages as low signal amplification and short residence time at the target site.[13,14] Nanotechnology-based nanoprobes have obvious advantages over small-molecule probes, such as

Received: 6 September 2021
Accepted: 17 February 2022
Published: 2 April 2022

larger specific surface area for modification of probe molecules, and the enhanced permeability and longer retention effect on tumors.[15,16] Consequently, the development of intelligent nanocarriers that integrate diagnosis and treatment is of great significance for cancer treatment.

Dicyanomethylene-4*H*-pyran (DCM), a hydrophobic NIR dye, has its fluorescence quenched when the $–NH_2$ terminal is occupied and restored when the $-NH_2$ terminal is free.[17–19] As such, the disulfide bond modifies thye DCM. DCM is released and activated when the disulfide bond is reduced and broken by the high concentration of GSH in tumor tissue. Disulfide-modified DCM can be used as a fluorescent probe to construct GSH stimulation–responsive tumor-imaging systems. Polydopamine (PDA) has been widely used in the construction of multifunctional nanocarriers because of its good biocompatibility, material stability, loading capability, and biodegradability.[20–22] The pyrocatechol group of PDA can be oxidized to pyroquinone, which can react with the nucleophilic group (such as amino or mercapto) in the form of Michael addition or Schiff-base reaction, making it valuable for further modification like loading anchors for specific recognition by the targeted receptor or a starting point for other covalent bonds.[23–25] It has been demonstrated that PDA-derived nanoparticles (NPs) display high drug-loading capability and good application prospects in the area of chemotherapy materials.[26,27]

Targeted drug delivery can be realized with the help of specific recognition like sugar–lectin interaction.[28,29] Carbohydrates, excellent biocompatible hydrophilic blocks, have received much attention for tumor-cell targeting on account of the fact that malignant cells are often accompanied by abnormal glycoprotein (lectin) content on cell surfaces, such as overexpressed asialoglycoprotein receptors (ASGP-Rs) on liver cancer cells.[30–32] Saccharides, such as *N*-acetyl galactosamine, β-D-galactose, and lactose derivatives can be modified for NP transport as active targeting ligands to enhance cellular uptake essay, thus improving the anticancer efficiency of multifunctional nanocarriers.[33–36]

Herein, we report a multifunctional glyco-NP PLDD (PDA@Lac/DCM/DOX) with activatable NIR probes for tumor imaging and targeted drug delivery. Disulfide-functionalized DCM (DCM-SS-NH_2) and amino-functionalized lactose (Lac-NH_2) were modified and loaded onto the surfaces of PDA NPs by Michael addition or Schiff-base reaction as GSH stimulation–responsive fluorescent probes and tumor-targeting moieties, respectively. Doxorubicin (DOX), a model anticancer drug, was loaded onto PLD NPs to obtain DOX-loaded PLD NPs (PLDD NPs) through π–π interactions directly (Scheme 1). The NIR probe DCM-SS-NH_2 can respond to the high concentration of GSH inside cancer tissue. We expected that these PLDD NPs would be able to achieve tumor imaging and targeted drug delivery.

Methods

All chemicals from commercial sources were used as received. Sodium methoxide, 4-acetamidobenzaldehyde, sodium azide, 1-(3-dimethylaminopropyl)-3-ethylcarbodiimide hydrochloride, D-lactose monohydrate, dopamine hydrochloride, and 2-[2-(2-chloroethoxy)ethoxy]ethanol were provided by Aladdin Reagent, 2'-hydroxyacetophenone and malononitrile were provided by Macklin Biotech, trifluoroacetic acid was provided by Dingxian Biotech, 3,3'-thiodipropionic acid and 1,1'-carbonyldiimidazole were provided by Energy Chemical Technology, and bis(trichloromethyl) carbonate, *N*-hydroxysuccinimide, and DOX hydrochloride were provided by Heowns Biotech. Normal liver cells (HL7702) and human hepatoma cells (HepG2) were supplied by Keygem Biotech (Nanjing, China) and cultured at 37°C and 5% CO_2 in 1640 medium (Gibco, USA) containing 10% FBS (Procell, China) and 100 U/mL penicillin–streptomycin (Solarbio, China).

A nuclear magnetic resonance spectrometer was given by Bruker (Karlsruhe, Germany) in deuterium reagents. The morphology of different kinds of PDA NPs was observed via a FEI S450 scanning electron microscopy (SEM). Ultraviolet-visible (UV-vis) spectra were obtained using a PerkinElmer Lambda 25 spectrophotometer and fluorescence spectra using a PerkinElmer LS-55. Imaging and targeting ability of cell lines were analyzed by a laser-scanning confocal microscope (Leica TCS SP8) and a flow cytometer (BD FACSAria III). MTT assays were used for the measurement of cell viability with a microplate reader (Tecan Infinite M1000 Pro, Switzerland).

Preparation and Characterization of PLD NPs

Synthesis of Lac-NH_2 (5), DCM-SS-NH_2 (13) and PDA is illustrated in Scheme S1–S4. Synthesis of PLD was conducted as follows. In a standard fabrication, 40 mg Lac-NH_2 (5) dispersed in 4 mL Tris-HCl (pH 8.5, 10 mM) was mixed with 1

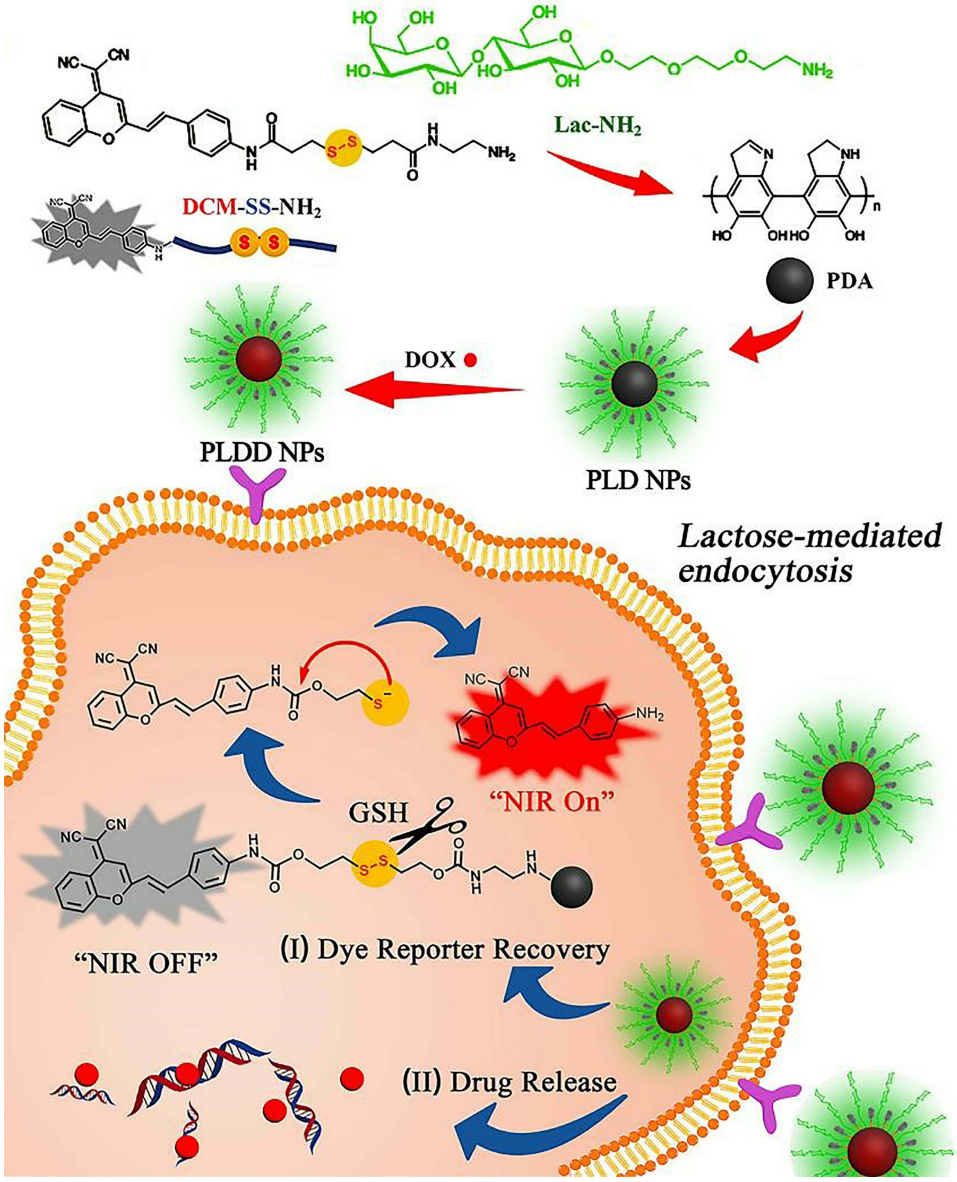

Scheme 1 Schematic illustration of the construction of PLDD NPs and the application for tumor imaging and targeted drug delivery.

mL PDA NP dispersion (10 mg/mL) under mild stirring, and the loading reaction proceeded at room temperature for 8 hours. Then, PDA-Lac NPs were collected via centrifugation (16,000 rpm, 10 minutes) and washed with 3 mL distilled water twice. The supernatant was collected, and dried to obtain the mass of Lac-NH_2 that had not reacted to the PDA. The precipitate was dispersed in Tris-HCl (pH 8.5, 10 mM, 9 mL) for the following application. DCM-SS-NH_2 (13) 55 mg was dissolved in a small amount of DMSO solution and then dispersed in 1 mL Tris-HCl (pH 8.5, 10 mM). The DMSO–Tris-HCl system was added dropwise to the PDA-Lac dispersion (9 mL) and stirred for 8 hours at room temperature. PLD NPs were obtained via centrifugation (16,000 rpm, 15 minutes) and washed with DMSO–Tris-HCl three times. A standard curve for DCM-SS-NH_2 was obtained (Supplementary Figure S14). The loading ratio of the Lac-NH_2 and DCM-SS-NH_2 was calculated according to the following equations. PLD NPs were resuspended in PBS (pH 7.4, 10 mM) for further use.

$$\text{Loading ratio (\%)} = (\text{mLac-NH}_2 \text{ loaded/mPLD}) \times 100\% \quad \text{(Eq. 1)}$$

where mLac-NH_2 loaded and mPLD refer to the mass of Lac-NH_2 encapsulated in PLD and the mass of PLD, respectively.

Loading ratio (%) = (mDCM-SS-NH_2 loaded/mPLD) × 100% (Eq. 2)

where mDCM-SS-NH_2 loaded and mPLD refer to the mass of DCM-SS-NH_2 encapsulated in PLD and the mass of PLD, respectively.

Loading Capacity and Release Profiles of PLDD NPs

Drug-loaded PDA NPs were prepared by incubating the prepared PLD NPs (5 mg) and DOX (25 mg) in 5 mL PBS (pH 7.4) for 12 hours at room temperature. The PLD NPs were separated by centrifugation (16,000 rpm, 15 minutes), then washed with PBS three times. The final product of PLD NPs was suspended in 5 mL PBS for further use (1 mg/mL). After the reaction between PLD and DOX, PLDD NPs were washed with PBS (pH 7.4, 10 mM) several times. The concentration of unloaded DOX in the supernatant was measured with UV-vis spectrophotometry at λ=490 nm. The interaction between PLD NPs and DOX was confirmed via FT-IR, UV-vis, and fluorescence spectra.

For measurements of drug release, 10 mg PLD NPs was dispersed by ultrasound in 1 mL PBS (pH 7.4, 10 mM), then distributed to three dialysis bags (molecular weight cut off 8,000 Da) and stirred in 10 mL PBS (pH 7.4, 10 mM). Testing medium (0.1 mL) was used to measure the amount of DOX released at λ=490 nm every 8 hours. Drug release at pH 5 was tested with the same method. The concentration of DOX was calculated:

$$C_{Dox}(\%) = \frac{M_T - M_S}{M_P + M_T - M_S} \times 100\%$$

where M_T is the total amount of DOX, M_S the content of free DOX in the supernatant, and M_P the quantity of PLD NPs.

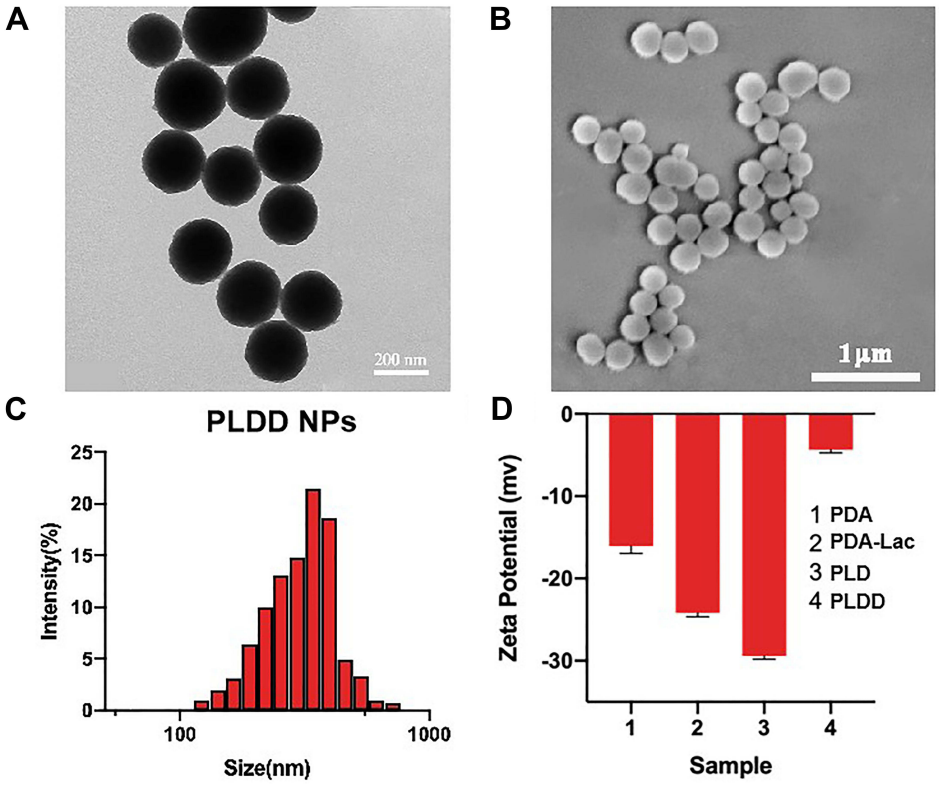

Figure 1 (A) TEM image of PDA NPs; **(B)** SEM image of PLDD NPs; **(C)** the size distribution of PLDD NPs by DLS; and **(D)** Zeta potential of PDA, PDA-Lac, PLD and PLDD NPs, respectively.

Free-Dye Release of PLD Mediated by Extra GSH

PLD NPs (DCM 2 mM) were dispersed in 5 mL DMSO–PBS (v:v 1:1), then 3 mL DMSO–PBS solution containing GSH (5 mM) was added and stirred for 2 hours (37°C). Fluorescence intensity of the medium at λ=650 nm was measured every half an hour.

Intracellular Monitoring and Fluorescence Recovery of PLD NPs

Fluorescein sodium (NaFL), a green hydrophilic fluorescent molecule, was chosen to take the place of DOX to avoid fluorescence overlap with DCM. HepG2 and HL7702 cells were cultured for 24 hours (37°C, 5% CO_2) in laser confocal dishes. Then, the original medium was replaced with medium containing PLD–NaFL (PLDN) NPs (1 mg/mL). HepG2 cells and HL7702 cells were cultured for another 24 hours after one group of HepG2 cells had been incubated with LBA for 4 hours in advance. The intracellular monitoring ability of PLD NPs was measured with CLSM.

Cell Culture and Cell Viability

HepG2 and HL7702 cells were selected to evaluate anticancer efficacy and cytotoxicity. RPMI 1640 medium was used to culture the HL7702 cells. FBS and penicillin–streptomycin were used in all culture media at concentrations of 10% and 1%, respectively.

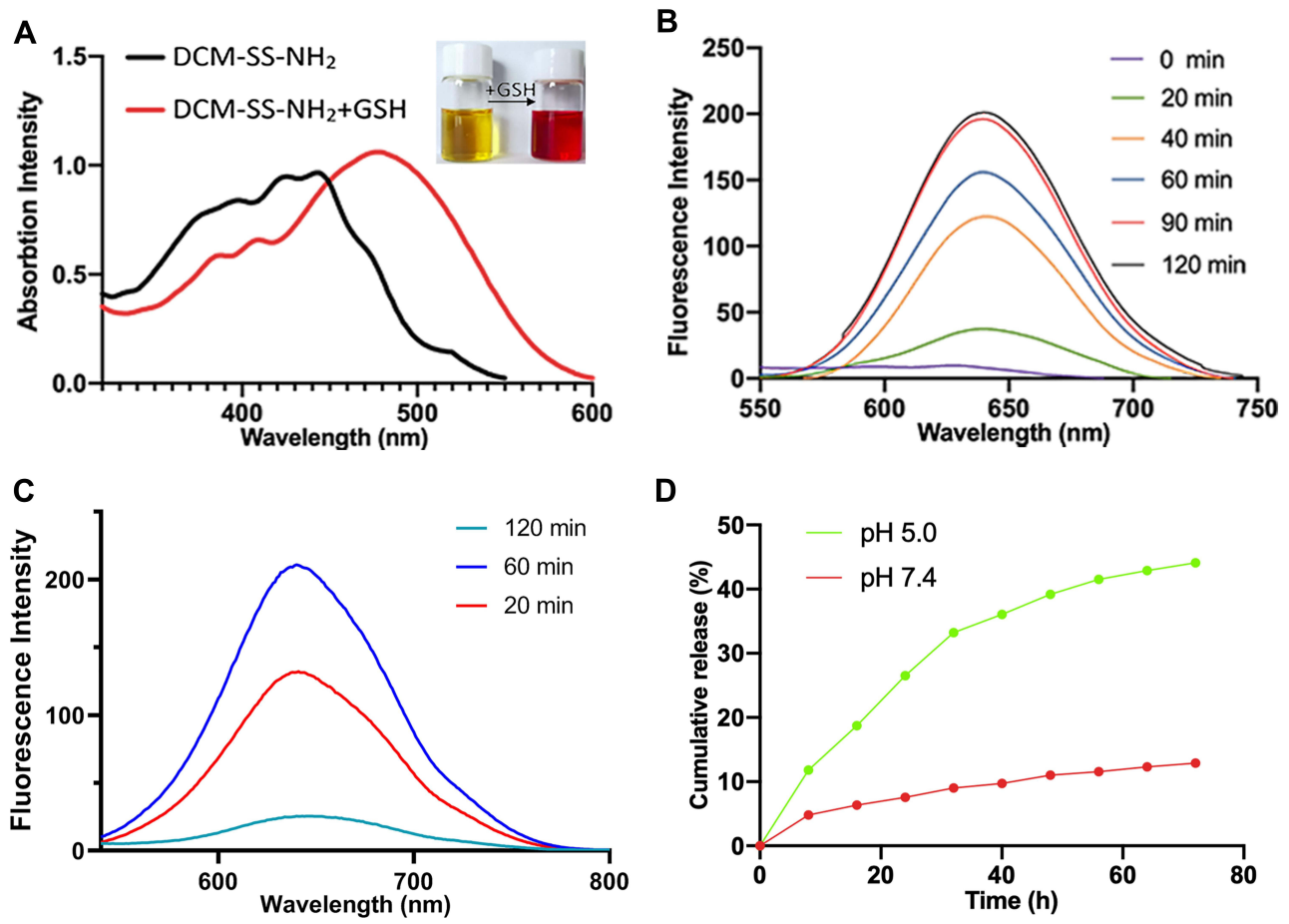

Figure 2 (A) The absorption spectra of DCM-SS-NH2 and DCM-SS-NH2 incubated with GSH (5 mM, 2 h); Emission spectra of DCM from DCM-SS-NH2 **(B)** and PLD NPs **(C)** incubated with GSH in DMSO/PBS solution (v/v, 1/1, DCM 20 μM) at 37°C during 2 h, λex= 490 nm, λem= 650 nm; **(D)** The cumulative drug release (%) of PLDD NPs during 72 h in phosphate buffer solution (pH 5.0, 7.4), respectively.

Results and Discussion

Synthesis and characterization details of Lac-NH_2 and DCM-SS-NH_2 can be seen in Supplementary Figure S1–S13. Using the aforementioned methods, we successfully prepared PLDD NPs. As shown in Figure 1, the spherical morphology of PDA and PLDD NPs was captureded by TEM and SEM. The average diameter of PDA and PLDD was 160±2.8 nm and 200±2.1 nm, respectively. The obvious Tyndall effect proved the existence of PLDD NPs (Supplementary Figure S15A). The size distribution and ζ-potential of PDA NPs were measured with dynamic light scattering (DLS). Supplementary Figures S15B and 1C show DLS curves for PLDD and PDA NPs: the average size of PDA and PLDD NPs was 260 and 340 nm, respectively, displaying good dispersibility. The different experimental conditions likely resulted in discrepancies in NP diameter measured by DLS vs SEM/TEM (an aqueous solution for DLS as opposed to a solid state under vacuum for SEM/TEM). In addition, the ζ-potentials of PDA, PDA-Lac, PLD, and PLDD NPs were −16.06, −24.2, −29.4, and −4.4 mV, respectively (Figure 1D). The negative potential of PDA, PDA-Lac, and PLD NPs was associated with the –OH, –CN, and catechol groups, and the decrease of negative potential of PLDD NPs was associated with the cationic molecule of DOX demonstrating the step-by-step synthesis of PLDD NPs. The load ratios for Lac-NH_2 and DCM-SS-NH_2 on the PLD NPs were 21.5% and 13.2%, respectively.

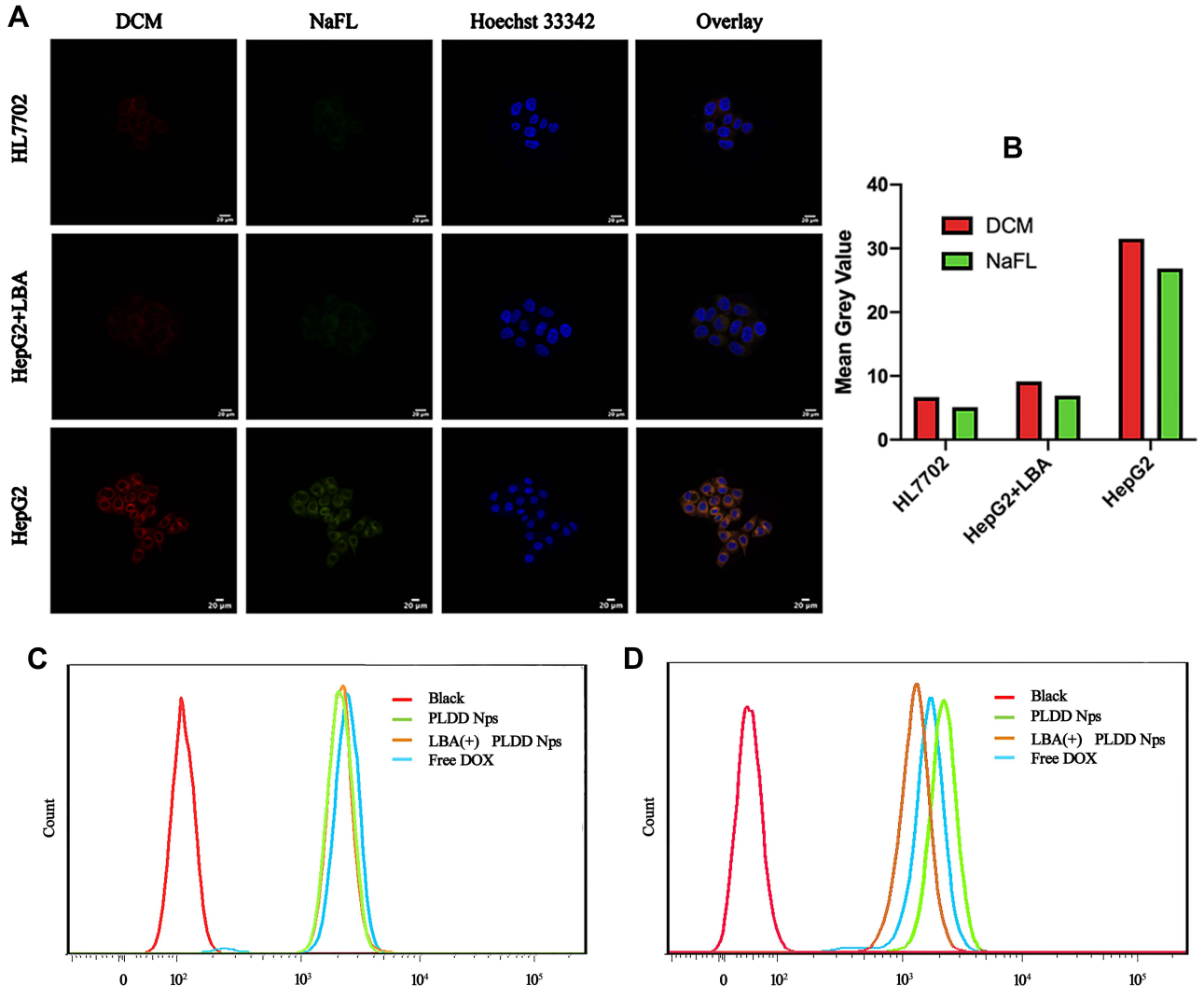

Figure 3 (A) CLSM images of HL7702 cells, HepG2 cells pre-treated with LBA and HepG2 cells cultured with PLD NPs (1 mg mL-1) for 4 h, respectively. The scale bar is 20 μm; **(B)** The average fluorescence intensity of different groups of cells; The cell uptake in HL7702 cells **(C)** and HepG2 cells **(D)** under different conditions measured by flow cytometry.

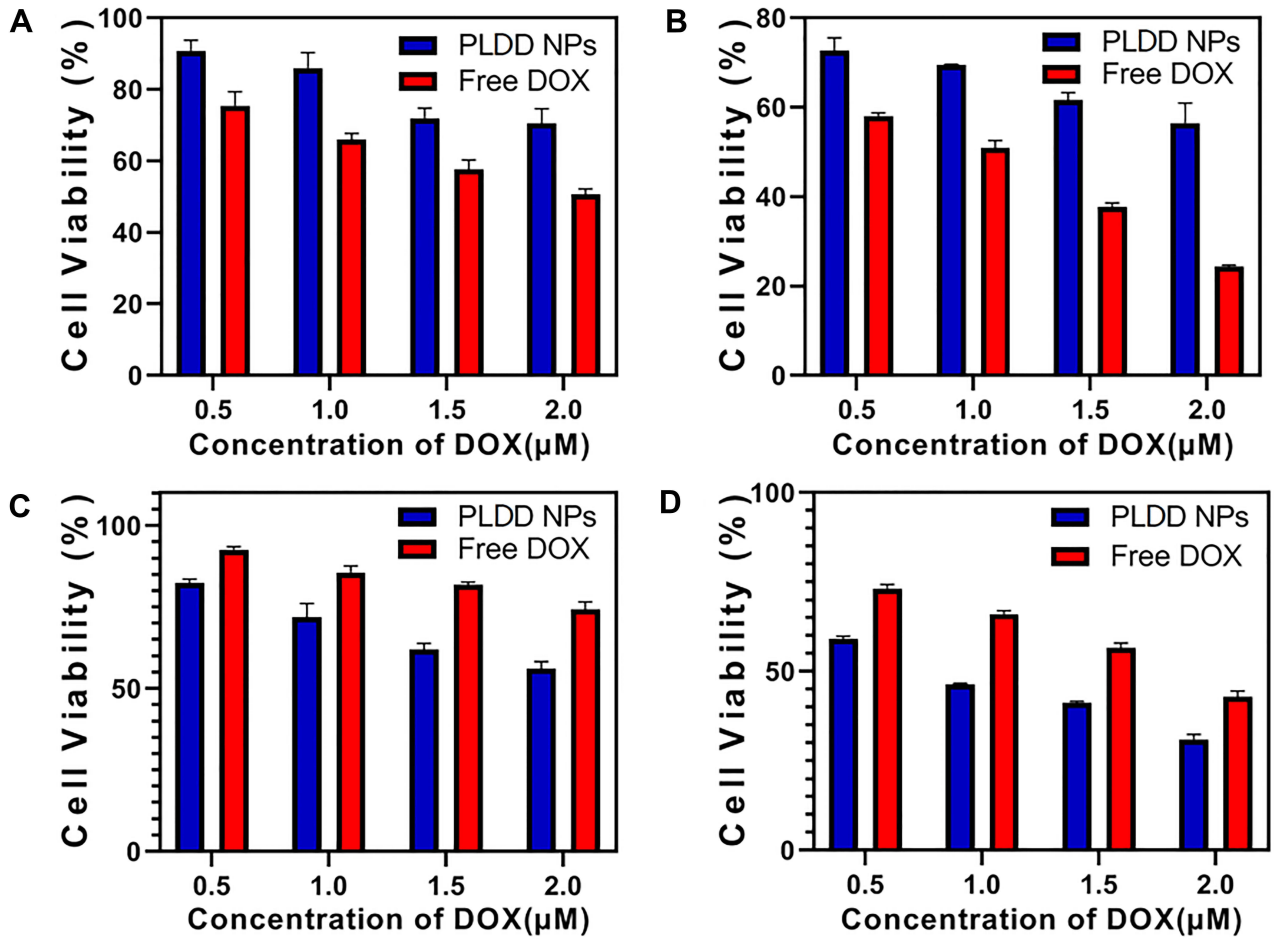

Figure 4 (A-B) HL7702 cells incubated with different concentrations of PLDD NPs and free DOX for 24 h, 48 h, respectively. **(C-D)** HepG2 cells incubated with different concentrations of PLDD NPs and free DOX for 24, 48 h, respectively.

NIR fluorescence of DCM probe was investigated with fluorescence spectrophotometry. For the NIR probe DCM-SS-NH_2, the colour of solution containing DCM-SS-NH_2 changed from yellow to red (Figure 2A) after incubation with extra GSH (5 mM), indicating the release of DCM through the reduction of disulfide bonds. NIR restoration and absorption spectra of DCM are shown in Figure 2B and Supplementary Figure S16. There were strong emission peaks at 650 nm with increased fluorescence intensity and strong absorption peaks at 490 nm and increased absorption intensity during the 2-hour incubation with GSH (5 mM), confirming the release of DCM via the cleavage of disulfide bonds by reaction with GSH. Strong emission peaks of DCM released from PLD NPs were detected (Figure 2C), indicating that PLD NPs could be used as nanoprobes for intracellular imaging. DOX loading was confirmed by fluorescence measurement, and was 49.57%. As shown in Supplementary Figure S17, the fluorescence of DOX on PDA NPs was quenched completely due to the photoinduced electron-transfer effect between DOX and PDA. As shown in Figure 2D, there was only a small amount of DOX released in the neutral environment (pH 7.4), while the amount released in the weak-acid environment (pH 5) was 44% after 72 hours, thus reducing cytotoxicity to normal cells.

CLSM indicated that the PLD NPs entered HepG2 cells easily. Meanwhile, the quenched fluorescence of DCM was restored in the cytoplasm, due to cracking of the disulfide bond exposed to the high concentration of GSH (Figure 3A). Merging of the red NIR fluorescence of DCM (λ_{em}=650 nm) and the green signal of NaFL (λ_{em}=512 nm) and then colocalization was indicated by the yellow areas. There was significant fluorescence enhancement in HepG2 cells compared with HL7702 cells, with the former preincubated with lactobionic acid (LBA, 2 mg/mL, Figure 3B), confirming the targeting ability of PLD NPs to HepG2 cells. The prepared NPs entered cells via galectin-mediated endocytosis.

The overexpressed ASGP-Rs existed in cell membrane of HepG2 cells, which can be specifically recognized by Lac-NH_2, a derivative of D-(+)-lactose. As shown in Figure 3C–D, there was an apparent decrease in cellular uptake efficiency in HepG2 cells on account of preincubation with LBA (2 mg/mL), thus indicating that Lac-NH_2 works as an active targeting ligand to specifically interact with ASGP-Rs via a lactose-mediated active process, and that LBA led to occupation of the lactose receptor, which subsequently inhibited lactose-mediated endocytosis. As a result, HL7702 cell group and LBA-treated HepG2 cell group showed only aspecific endocytosis of NPs.

In order to demonstrate anticancer activity, the cytotoxicity of PLDD NPs was studied using MTT assays. As shown in Supplementary Figure S18, PLD NPs showed negligible cytotoxicity to HL7702 cells after 48 hours, indicating that PLD NPs had good biocompatibility. The relative viability of HL7702 cells after being cultured with PLDD NPs for 24 and 48 hours was higher than cells cultured with free DOX (Figure 4A and B). On the contrary, HepG2 cells under the same treatments displayed lower viability after cocultured with PLDD NPs than with free DOX (Figure 4C and D). These results indicated that PLDD NPs enhanced drug uptake via specific recognition of ASGP-Rs and improve anticancer efficacy in HepG2 cells, as well as reducing the side effects on normal cells.

Conclusion

In this work, we successfully constructed multifunctional nanocarriers, PLDD NPs, composed of a DCM-SS-NH_2 moiety as an active NIR probe, lactose derivative Lac-NH_2 as a hepatoma-targeting ligand, and drug carrier PDA NPs. PLD NPs displayed good biocompatibility and HepG2-targeting ability due to the special recognition between the lactose derivative of NPs and overexpressed ASGP-Rs on HepG2 cell membrane. More importantly, the disulfide bond of DCM-SS-NH_2 was broken by the high concentration of GSH inside cancer cells, activating the NIR fluorescence probe DCM for cancer-cell imaging. PLDD NPs also exhibited higher anticancer efficiency on HepG2 cells and reduced side effects on normal cells compared with free DOX. Therefore, this PLDD nanocarrier has provided a great example for both tumor imaging and targeted drug delivery.

Acknowledgments

This work was supported by the National Natural Science Foundation of China (21877088, 21772157). The authors thank the Teaching and Research Core Facility at the College of Life Science and Life Science Research Core Services, Northwest A&F University for helping with characterizations including SEM, TEM, CLSM, and flow cytometry.

Disclosure

The authors report no conflicts of interest in this work.

References

1. Shen Y, Friend CS, Jiang Y, et al. Nanophotonics: interactions, materials, and applications. *J Phys Chem B*. 2000;104(32):4–5. doi:10.1021/jp0031395
2. Cui H, Hu D, Zhang J, et al. Gold nanoclusters-indocyanine green nanoprobes for synchronous cancer imaging, treatment, and real-time monitoring based on fluorescence resonance energy transfer. *ACS Appl Mater Inter*. 2017;9(30):25114–25127. doi:10.1021/acsami.7b06192
3. Poplinger D, Bokan M, Hesin A, et al. Ratiometric fluorescence monitoring of antibody-guided drug delivery to cancer cells. *Bioconjugate Chem*. 2021;32(8):1641–1651. doi:10.1021/acs.bioconjchem.1c00205
4. Chao S, Lv X, Ma N, et al. A supramolecular nanoprodrug based on a boronate ester linked curcumin complexing with water-soluble Pillar[5]arene for synergistic chemotherapies. *Chem Commun*. 2020;56(62):8861–8864. doi:10.1039/D0CC04315J
5. Sun G, Zuo M, Qian W, et al. Highly efficient artificial light-harvesting systems constructed in aqueous solution for supramolecular photocatalysis. *Green Synth Catal*. 2021;2(1):32–37. doi:10.1016/j.gresc.2021.01.003
6. Feng W, Jin M, Yang K, et al. Supramolecular delivery systems based on pillararenes. *Chem Commun*. 2018;54(97):13626–13640. doi:10.1039/C8CC08252A
7. Owens EA, Henary M, El Fakhri G, et al. Tissue-specific near-infrared fluorescence imaging. *Accounts Chem Res*. 2016;49(9):1731–1740. doi:10.1021/acs.accounts.6b00239
8. Zhao Y, Hai Z, Wang H, et al. Legumain-specific near-infrared fluorescence "Turn On" for tumor-targeted imaging. *Anal Chem*. 2018;90(15):8732–8735. doi:10.1021/acs.analchem.8b02704
9. Ji Y, Jones C, Baek Y, et al. Near-infrared fluorescence imaging in immunotherapy. *Adv Drug Deliver Rev*. 2020;167:121–134. doi:10.1016/j.addr.2020.06.012
10. Zhu H, Li Q, Shi B, et al. Dual-emissive platinum(II)metallacage with a sensitive oxygen response for imaging of hypoxia and imaging-guided chemotherapy. *Angew Chem Int Ed*. 2020;132(45):20383–20389. doi:10.1002/ange.202009442

11. Song N, Zhang Z, Liu P, et al. Pillar[5]arene-modified gold nanorods as nanocarriers for multi-modal imaging-guided synergistic photodynamic-photothermal therapy. *Adv Funct Mater*. 2021;31(21):2009924. doi:10.1002/adfm.202009924
12. Zhou W, Chen Y, Yu Q, et al. Ultralong purely organic aqueous phosphorescence supramolecular polymer for targeted tumor cell imaging. *Nat Commun*. 2020;11(1):1–10. doi:10.1038/s41467-020-18520-7
13. Liu Z, Wang B, Ma Z, et al. Fluorogenic probe for the human ether-a-go-go-related gene potassium channel imaging. *Anal Chem*. 2015;87(5):2550–2554. doi:10.1021/ac504763b
14. Mu J, Liu F, Rajab MS, et al. A small-molecule FRET reporter for the real-time visualization of cell-surface proteolytic enzyme functions. *Angew Chem Int Ed*. 2014;53(52):14357–14362. doi:10.1002/anie.201407182
15. Xing Y, Zhao J, Conti PS, et al. Radiolabeled nanoparticles for multimodality tumor imaging. *Theranostics*. 2014;4(3):290–306. doi:10.7150/thno.7341
16. Wang Y, Jiang Y, Zhang M, et al. Protease-activatable hybrid nanoprobe for tumor imaging. *Adv Funct Mater*. 2001;24(34):5443–5453. doi:10.1002/adfm.201400419
17. Shang L, Bian T, Zhang B, et al. Inside cover: graphene-supported ultrafine metal nanoparticles encapsulated by mesoporous silica: robust catalysts for oxidation and reduction reactions. *Angew Chem Int Ed*. 2014;53(1):2. doi:10.1002/anie.201310508
18. Cao S, Pei Z, Xu Y, et al. Glyco-nanovesicles with activatable near-infrared probes for real-time monitoring of drug release and targeted delivery. *Chem Mater*. 2016;28(12):4501–4506. doi:10.1021/acs.chemmater.6b01857
19. Guo Z, Zhu W, Tian H. Dicyanomethylene-4H-pyran chromophores for OLED emitters, logic gates and optical chemosensors. *Chem Commun*. 2012;48(49):6073–6084. doi:10.1039/c2cc31581e
20. Wu R, Wang H, Hai L, et al. A photosensitizer-loaded zinc oxide-polydopamine core-shell nanotherapeutic agent for photodynamic and photothermal synergistic therapy of cancer cells. *Chin Chem Lett*. 2020;31(1):189–192. doi:10.1016/j.cclet.2019.05.004
21. Feng J, Yu W, Xu Z, et al. An intelligent ZIF-8-gated polydopamine nanoplatform for in vivo cooperatively enhanced combination phototherapy. *Chem Sci*. 2020;11(6):1649–1656. doi:10.1039/C9SC06337D
22. Zhang Y, Wu X, Hou C, et al. Dual-responsive dithio-polydopamine coated porous CeO_2 nanorods for targeted and synergistic drug delivery. *Int J Nanomed*. 2018;13:2161–2173. doi:10.2147/IJN.S152002
23. Liu Y, Ai K, Lu L. Polydopamine and its derivative materials: synthesis and promising applications in energy, environmental, and biomedical fields. *Chem Rev*. 2014;114(9):5057–5115. doi:10.1021/cr400407a
24. Li Y, Dai H, Zhang Q, et al. In situ generation of electron acceptor to amplify the photoelectrochemical signal from poly (dopamine)-sensitized TiO_2 signal crystal for immunoassay. *J Mater Chem B*. 2016;4(15):2591–2597. doi:10.1039/C5TB02525G
25. Ball V, Del Frari D, Toniazzo V, et al. Kinetics of polydopamine film deposition as a function of pH and dopamine concentration: insights in the polydopamine deposition mechanism. *J Colloid Interf Sci*. 2012;386(1):366–372. doi:10.1016/j.jcis.2012.07.030
26. Chen X, Huang Y, Yang G, et al. Polydopamine integrated nanomaterials and their biomedical applications. *Curr Pharm Design*. 2015;21(29):4262–4275. doi:10.2174/1381612821666150901103418
27. Kwon IS, Bettinger CJ. Polydopamine nanostructures as biomaterials for medical applications. *J Mater Chem B*. 2018;6(43):6895–6903. doi:10.1039/C8TB02310G
28. Chang Y, Yang K, Wei P, et al. Cationic vesicles based on amphiphilic pillar[5]arene capped with ferrocenium: a redox-responsive system for drug/siRNA co-delivery. *Angew Chem Int Ed*. 2014;53(48):13126–13130. doi:10.1002/anie.201407272
29. Lu Y, Hou C, Ren J, et al. A multifunctional supramolecular vesicle based on complex of cystamine dihydrochloride capped pillar[5]arene and galactose derivative for targeted drug delivery. *Int J Nanomed*. 2019;14:3525–3532. doi:10.2147/IJN.S191256
30. Liu S, Huang Y, Chen X, et al. Lactose mediated liver-targeting effect observed by ex vivo imaging technology. *Biomaterials*. 2010;31(9):2646–2654. doi:10.1016/j.biomaterials.2009.12.019
31. Chao S, Shen Z, Pei Y, et al. Pillar[5]arene-based supramolecular photosensitizer for enhanced hypoxic-tumor therapeutic effectiveness. *Chem Commun*. 2021;57(62):7625–7628. doi:10.1039/D1CC02959B
32. Hou C, Ma N, Shen Z, et al. A GSH-responsive nanoprodrug system based on self-assembly of lactose modified camptothecin for targeted drug delivery and combination chemotherapy. *Int J Nanomed*. 2020;15:10417–10424. doi:10.2147/IJN.S276470
33. Yang R, Meng F, Ma S, et al. Galactose-decorated cross-linked biodegradable poly (ethylene glycol)-b-poly (ε-caprolactone) block copolymer micelles for enhanced hepatoma-targeting delivery of paclitaxel. *Biomacromolecules*. 2011;12(8):3047–3055. doi:10.1021/bm2006856
34. Ding Y, Wei J, Li S, et al. Host–guest interactions initiated supramolecular chitosan nanogels for selective intracellular drug delivery. *ACS Appl Mater Inter*. 2019;11(32):28665–28670. doi:10.1021/acsami.9b09059
35. Xie J, Lu Y, Yu B, et al. Galactose-modified enzymatic synthesis of poly (amino-co-ester) micelles for co-delivery miR122 and sorafenib to inhibit hepatocellular carcinoma development. *Chin Chem Lett*. 2020;31(5):1173–1177. doi:10.1016/j.cclet.2019.10.030
36. Yang K, Pei Y, Wen J, et al. Recent advances in pillar[n]arenes: synthesis and applications based on host-guest interactions. *Chem Commun*. 2016;52(60):9316–9326. doi:10.1039/C6CC03641D